Electron Spin Resonance and Molecular Oribtal Study of One-Electron-Reduced *O,O′*-Diphenylenehalonium Cations: First Evidence for a Diaryliodine Radical, $Ar_2I^{\bullet}$ or Simply a New σ^*-Radical?

Yurii V. Razskazovskii,[†] Michael J. Raiti, and Michael D. Sevilla*

Department of Chemistry Oakland University Rochester, Michigan 48309-4401

Received: April 19, 1999

One-electron reduction of *o,o′*-diphenylenebromonium (DPB) and *o,o′*-diphenyleneiodonium (DPI) cations in low-temperature glasses produces free radical intermediates whose halogen hyperfine couplings suggest significant spin densities on bromine (0.13) and iodine (0.30). An adequate theoretical description of these species has been obtained at both semiempirical (PM3) and density functional levels of theory. These calculations show these species are a planar conformation of the 2-halobiphenyl-2′-yl radicals, stabilized through intramolecular three-electron (or σ^*) carbon−halogen bonding. Theory also predicts a nonequivalence of the C−X bonds and unsymmetrical spin density distribution over the two C−X bonding carbons. As compared to DPB, the DPI radical gives evidence for more equivalent bonding of the iodine to both carbons, accompanied by lower potential barriers for intramolecular iodine atom migration (1−2 kcal mol^{-1}) along the σ^*-bond. In the case of 3-nitrosubstituted DPI (NDPI) the one-electron-reduced intermediate was observed both as a σ^*-radical (in polar glasses) and as a π^*-radical (when intercalated into DNA). Calculations suggest that the change from σ^* to π^* on intercalation into DNA is driven both by electric field of the DNA backbone and by π-stacking of NDPI with DNA bases. One-electron-reduced diphenylenehalonium derivatives were not found to undergo intramolecular free radical addition leading to a cyclohexadienyl-type adduct. This result is supported by theoretical calculations indicating that such a process would be endothermic by 13.9 kcal mol^{-1} at the ROMP2/6-31G* level.

Introduction

o,o′-Diphenylenehalonium cations (DPH) are of considerable interest as they are able to intercalate into DNA and potentiate DNA damage.[1] For example, reduction of DPH by solvated electrons generated by ionizing irradiation forms reactive radical species that are found to abstract hydrogen from the sugar−phosphate backbone.[1] This is potentially a biologically important process in which a reducing entity (e.g., the solvated electron) is transformed into oxidative DNA damage. The classical and, to the best of our knowledge, the only earlier example of compounds acting in a similar manner are 5-halogen-substituted uracils (primarily bromo- and iodo-derivatives) that substitute for thymine in the DNA structure.[2] These compounds, when incorporated in DNA, cleave DNA through a mechanism that begins with electron capture. The electron adduct rapidly dehalogenates, forming the reactive uracil-5-yl radical, which then abstracts a hydrogen atom from the DNA sugar−phosphate backbone.[3,4] Abstraction of hydrogen from the DNA backbone in most cases leads to a DNA strand break.[2,5]

A similar mechanism involving a biphenyl-2-yl radical as a hydrogen-abstracting intermediate has been suggested for the DPH-mediated cleavage of DNA.[1] However, an important difference is that DPH cleaved DNA as external agents bound to DNA through intermolecular interactions and not through covalent incorporation into the strand. The binding characteristics and the UV−vis spectral changes on DPH association with DNA are consistent with intercalation as the most feasible binding mode.[6] Diphenylenehalonium cations are therefore the first DNA intercalators that are able to convert ionizing radiation's reductive pathway to an oxidative strand cleavage.

The mechanism by which a one-electron-reduced DPH results in a DNA strand break is of particular interest. The ESR spectra of one-electron-reduced *o,o′*-diphenylenebromonium (DPB) and *o,o′*-diphenyleneiodonium (DPI) cations detected in their complexes with DNA at low temperatures have indicated a substantial spin density on the halogens.[1] This raises a question as to whether these species represent the first directly observed example of hypervalent halogen derivatives of the general formula $R_2Hal^{\bullet}$. Such a species would be isoelectronic with known phosphoranyl $R_4P^{\bullet}$[7] and sulfuranyl $R_3S^{\bullet}$ radicals.[8] To the best of our knowledge, hypervalent halogen-centered species of this kind have not previously been observed, although their existence as bound states was suggested on the basis of circumstantial data.[9−11] This paper presents the first analysis of electronic structure of one-electron-reduced *o,o′*-diphenylenehalonium cations (DPH) based on experimental ESR evidence and quantum-chemical calculations.

Experimental Section

Materials. The DPH derivatives employed in this study are shown below. Four of them including DPB,[12] DPI,[13] NDPI,[14] and DNDPI[15] were synthesized from commercially available reagents following the literature procedures. The reduction of the nitro derivatives with $SnCl_2$ (1.5-fold excess over theoretical) in a concentrated hydrochloric acid/methanol mixture (1:2 v/v) at room temperature overnight yielded the corresponding amino derivatives, which were further purified by crystallization from

[†] Present address: Department of Biochemistry and Biophysics, Box 712, University of Rochester Medical Center, Rochester, New York 14642.

10.1021/jp991263m CCC: $18.00
Published on Web 07/20/1999

water. Diphenyliodonium chloride (Aldrich) and salmon testes DNA (Sigma) were used as received.

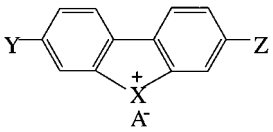

X	Y	Z	A	abbreviation
Br	H	H	Br	DPB
I	H	H	Cl	DPI
I	NH_2	H	Cl	ADPI
I	NO_2	H	HSO_4	NDPI
I	NO_2	NO_2	HSO_4	DNDPI

Instrumentation. γ-irradiations were performed using a ^{60}Co source (US Nuclear Model GR9) with the dose rate 3.5 kGy/h. Absorption spectra were recorded on Milton Roy 3000 and Shimadzu UV160U spectrophotometers. ESR spectra were taken on a Varian E-Line Century Series X-band system equipped with a dual cavity and variable temperature accessories. Quantum chemical calculations were performed using the GAUSSIAN 94[16] and SPARTAN 5 program packages implemented on a Silicon Graphics Indigo R10000 computer.

Methods. *(a) Generation of One-Electron-Reduced Intermediates.* Ionizing irradiation combined with matrix isolation techniques have been employed to detect the primary products of one-electron reduction of halonium compounds. The solvents employed in this study as trapping matrixes (i.e., water, aqueous LiCl, and ethylene glycol mixtures with water and DMSO) are relatively inert toward radiation-produced electrons but efficiently immobilize the holes at 77 K in the form of $HO^{\bullet}$, Cl_2^- and carbon-centered radicals, respectively. At the concentrations employed in our studies the solutes react primarily with mobile electrons produced through ionization of the matrix. The irradiation doses applied to the polycrystalline aqueous samples were up to 2 Mrad, while the glassy samples were irradiated to the doses within the 0.4−0.7 Mrad range.

(b) ESR Measurements. The compounds sufficiently soluble in glass-forming solvents such as aqueous 6 M LiCl, 1:1 v/v ethylene glycol−water and 4:2.5 v/v DMSO−ethylene glycol mixture were studied in Suprasil ESR 3 mm i.d. tubes following conventional ESR procedures. A different procedure was applied to preparation of the DNA-containing samples. The additives were solubilized in 10 mL of 10 mM DNA (in bases) to saturation followed by filtration. The filtrates were lyophilized and soaked in 300 μL of D_2O (Aldrich, 99.5% D) forming gels containing approximately 10 wt % of DNA. The gels were frozen as approximately 10 mm long, 3 mm in diameter cylindrical plugs and handled as usual. All irradiations and measurements were performed at 77 K. The spectra were calibrated using the aqueous solution of the Fremy's salt (dipotassium nitrosodisulfonate) as a standard ($g = 2.0056$, a(N) = 13.09 G).

(c) Quantum-Chemical Calculations. All the structures were fully optimized unless otherwise mentioned in the text. Density functional calculations were performed at the pBP86/DN** level using the SPARTAN program package and at the B3LYP/6-31G* level using the GAUSSIAN 98 set of programs. The DN** basis set is equivalent to 6-31G**, and pBP has been shown to produce energy results comparable to those of B3LYP, although B3LYP was found to be superior for bond distances.[17] The restricted-open shell HF treatment was employed for both semiempirical and ab initio MO spin density calculations to avoid the substantial spin contamination found at the UHF level.

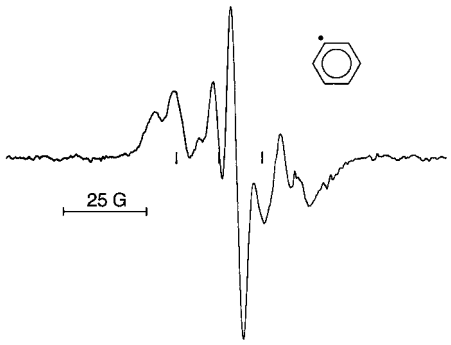

Figure 1. Electron spin resonance spectrum of one-electron-reduced Ph_2I^+ in 6 M LiCl. The spectrum shown is that of the phenyl radical and is evidence for reductive cleavage of the C−I bond. Three vertical risks in the middle of the spectra are the positions of Fremy salt resonances used for calibration (a(N) = 13.09 G, $g = 2.0056$).

Results

1. Primary Reduction Intermediates. *(a) Diphenyliodonium Cation.* We find that one-electron reduction of Ph_2I^+ in a 6 M LiCl glass gives rise to the persistent ESR signal at 77 K shown in Figure 1. The hyperfine structure of the spectrum shows two hydrogen couplings at 16 G and two smaller couplings at 6 G with a g value of 2.0025. These parameters are those expected for the phenyl radical in a glassy matrix.[18,19] Clearly, electron attachment results in a cleavage of the carbon halogen bond releasing the phenyl radical as shown in the reaction below:

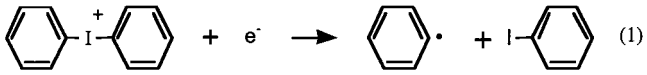

(1)

We find that detectable amounts of phenyl radicals are also generated from Ph_2I^+ in aqueous ethylene glycol glass**.** However, the phenyl radicals trapped in ethylene glycol decay on standing at 77 K likely through hydrogen abstraction from the matrix. ESR spectral features attributable to the hypothetical $Ph_2I^{\bullet}$ intermediate were not found in either LiCl or in ethylene glycol glasses. This suggests that reduction of Ph_2I^+ to form the acyclic $Ph_2I^{\bullet}$ species produces an intermediate that spontaneously decomposes even at 77 K.

(b) DPH Derivatives. We find that the reduction of DPB, DPI, and amino-substituted DPI's in ethylene glycol glasses result in stable intermediates at 77 K whose ESR spectra show characteristic ^{79,81}Br ($I = {}^3/_2$) or ^{127}I ($I = {}^5/_2$) anisotropic hyperfine features indicative of substantial spin densities on the halogens (Figure 2A,B). Therefore, one-electron reduction of these DPHs does not initially result in a carbon-centered 2′-halogenated biphenyl-2-yl radical expected by analogy with Ph_2I^+, but in a partially halogen-centered species. Such intermediates were previously reported in γ-irradiated DNA doped with either DPI or DPB.[1] The spectra (Figure 2A,B) are resolved enough to allow for determination of the anisotropic hyperfine coupling constants $A_{||}$, which include both isotropic and anisotropic contributions (Table 1):

$$A_{||} = a_{iso} + 2B$$

The corresponding $A_{\perp}$ values are not available since the appropriate hyperfine features are hidden under the matrix signal. Evaluation of the spin densities using $A_{||}$ alone can be performed only by making additional reasonable assumptions regarding the electronic structure of the intermediate. The ρ(X) values reported in Table 1 are based on the assumptions that the unpaired electron in $DPH^{\bullet}$ occupies a σ*-type SOMO as

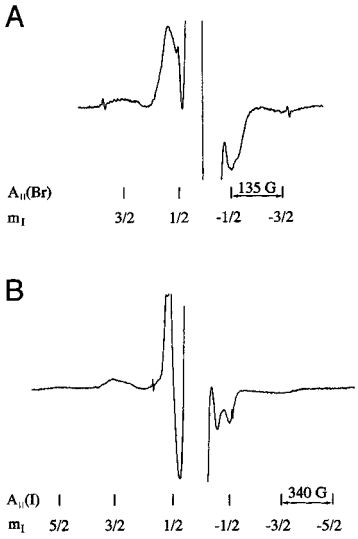

Figure 2. Electron spin resonance spectra of one-electron-reduced DPB (A) and DPI (B) in an ethylene glycol/water glass at 77 K. The parallel anisotropic hyperfine structure in the wings originates from the halogen nuclei and is marked by the stick diagrams.

TABLE 1: ESR Characteristics of One-Electron-Reduced DPH Derivatives (Z = H)

X	Y	matrix	$\|A_{\|\|}(X)\|$, G	$\rho(X)$	$\|A_{\|\|}(N)\|$, G
Br	H	EG[a]	135	0.15	
I	H	EG	340[d]	0.30	
I	NH_2	EG	340[d]	0.30	
I	NO_2	DMSO/EG[b]	340[d]	0.30	
I	NO_2	DNA/D_2O[c]	0		38 (^{15}N), 27 (^{14}N)

[a] Ethylene glycol/water 1:1 v/v. [b] DMSO/ethylene glycol 4:2.5 v/v. [c] 10 weight % of DNA in D_2O containing approximately one DPH cation per 5 DNA bases. [d] ±20 G.

indicated in the structure and that the ratio between $A_{||}$ and ρ-(X) in these species is the same as in other halogen-containing σ^*-radicals (see Discussion):

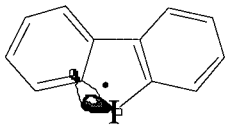

(2)

These assumptions allow the calculation of $\rho(X)$ in DPH$^\bullet$ using the spin densities and hyperfine couplings for Br_2^- (ρ-(Br) = 0.5, $A_{||}$(Br) = 460 G[20]) and I_2^- (ρ(I) = 0.5, a_{iso} = 207 G, B = 193 G[21]) as reference values. These values result in the following approximate relationships that estimate the spin density on the halogen given the experimental value of $A_{||}$ hyperfine couplings: $\rho(Br) = A_{||}(Br)/920$ and $\rho(I) = A_{||}(I)/1186$.

The spin densities reported in Table 1 indicate that, despite appreciable spin density on bromine, the DPB$^\bullet$ radical remains chiefly a carbon-based species. A substantially higher spin density on iodine of 0.3 in DPI electron adducts suggests stronger coupling between the carbon radical site(s) and the halogen. As can be seen from Table 1, amino substitution into the DPI core has no detectable effect on the spin density distribution in the reduced intermediates.

However, the situation is very different for the nitro derivative, NDPI. While NDPI irradiated in an ethylene glycol/DMSO glass produces the iodine-centered radical typical of other DPHs (Figure 3), irradiation of an NDPI−DNA complex in a frozen aqueous solution produces an ESR spectrum (Figure 4A) from a largely nitrogen-centered radical. This surprising result has

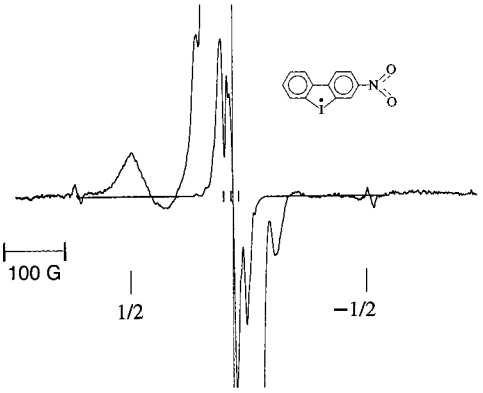

Figure 3. ESR spectrum of NDPI−^{14}N in ethylene glycol/DMSO glass at 77 K. The features labeled in the wings are from iodine hyperfine couplings expected for the iodonium radical.

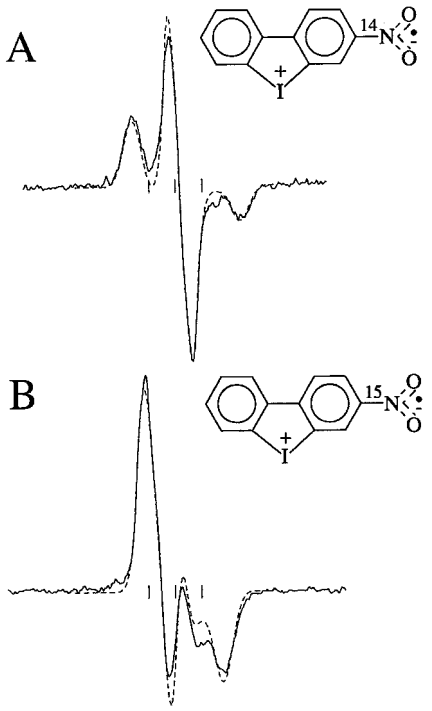

Figure 4. The ESR spectra of one-electron-reduced ^{14}N- and ^{15}N-labeled NDPI (A and B, respectively) detected in a frozen solution of DNA in D_2O (100 mg mL^{-1}) at 77 K. The solutions containing approximately 1 NDPI/5 DNA bases were irradiated to the dose 20 kGy at 77 K and annealed to 240 K to eliminate DNA radicals. Dashed lines show the results of the anisotropic spectrum simulation using the following set of parameters: (A) $g_{||}$ = 2.0022, $g_\perp$ = 2.0052, $a_{||}(^{14}N)$ = 76 MHz, $a_\perp(^{14}N)$ = 8 MHz; (B) $g_{||}$ = 2.0022, $g_\perp$ = 2.0052, $a_{||}(^{15}N)$ = 106.4 MHz, $a_\perp(^{15}N)$ = 11.2 MHz, line widths in parallel and perpendicular orientations 9 and 7 G, respectively. Three vertical risks in the middle of the spectra are the positions of Fremy salt resonances used for calibration (a(N) = 13.09 G, g = 2.0056)

been verified using ^{15}N-labeled NDPI (Figure 4B). Since ^{15}N has the nuclear spin of $I = {}^1/_2$, it should change the three-line ESR pattern of the ^{14}N-substituted species ($I(^{14}N) = 1$) into a two-line pattern for the ^{15}N system. In addition, the ratio of hyperfine coupling constants in the spectra of ^{15}N- and ^{14}N-labeled species must match the ratio of the correspondent nuclear g-factors, which is 1.404. A comparison of the ESR spectra obtained from ^{14}N- and ^{15}N-substituted NDPI−DNA complexes shows the expected spectral transformation on isotopic substitution with the appropriate ratio of hyperfine coupling constants (1.40), as confirmed by simulation (Figure 4A,B and Table 1). This unambiguously places a substantial spin density on nitrogen

of the nitro group while the lack of any ^{127}I hyperfine structure indicates no appreciable spin density on the iodine. Evidently, intercalation of NDPI into DNA radically changes the nature of electron spin distribution in one-electron-reduced NDPI. The results of theoretical calculations discussed later link this phenomenon to an inversion of the SOMO level from a σ^*-MO to a π^*-MO on NDPI binding to DNA.

2. Secondary Transformations. All one-electron-reduced DPH shows a much higher thermal stability than the phenyl radical both in aqueous LiCl or in ethylene glycol glass. Such stabilization obviously results from partial delocalization of the free spin from carbon onto bromine and iodine in one-electron-reduced DPH, which nature will be discussed later.

The DPB$^\bullet$ radical generated in 6 M LiCl glass at 77 K decays on annealing to temperatures above 130 K without detectable production of any new paramagnetic species. This species, therefore, shows no tendency to undergo intramolecular free radical addition on annealing, leading to a cyclohexadienyl-type adduct. This behavior is in sharp contrast with earlier reported reactivity of a phenyl radical/iodobenzene couple generated from Ph_2I^+ in the same matrix.[1] The latter readily transforms into the cyclohexadienyl radical on annealing just above 77 K. The results of theoretical calculations presented below clearly show that intramolecular formation of cyclohexadienyl adducts by one-electron-reduced DPH is prevented by the endothermicity of this process associated with the formation of a strained four-membered ring structure.

The ESR signal of DPB$^\bullet$ and DPI$^\bullet$ radicals trapped in aqueous ethylene glycol glass begins to disappear above 140 K. This process also does not result in formation of any new species in addition to the matrix radicals already present in the sample. Therefore, it is possible that both DPB$^\bullet$ and DPI$^\bullet$ decay in ethylene glycol glasses through hydrogen abstraction from the matrix, forming the matrix radical. Such a possibility is supported by our earlier finding that these species abstract hydrogen from DNA when generated in DPH−DNA complexes.[1] Unfortunately, no direct ESR evidence for hydrogen abstraction from ethylene glycol by DPH is available at this moment because the temperature-induced changes of the matrix signal itself mask the effect caused by DPH radicals.

3. Molecular-Orbital Calculations. Molecular orbital calculations were performed at density functional as well as semiempirical and ab initio levels of theory. These calculations have been employed to provide further insight into the structures of the primary reduction intermediates and their secondary transformations**.** Our previous work on halogen three-electron bonding has shown that the PM3 semiempirical treatment, density functional theory using the Spartan Code at the DN** level and ab initio calculations at the MP2/6-31G* level all gave good descriptions of chlorine three-electron bonding, although the semiempirical and DFT techniques slightly overemphasized the strength of the $\sigma\sigma^*$-bonding.[22] In this work we employ DFT calculations at the pBP86/DN** and B3LYP/6-31G* levels. The B3LYP and ab intio treatments could not be performed for the iodine containing species in this work owing to the lack of suitable basis sets in GAUSSIAN 98 for these atoms. Some calculations with the 3-21G* basis set were performed at the ROHF level. Results showed that these calculations do not give a proper theoretical description of three-electron bonding, as they invariably predict no substantial $\sigma\sigma^*$ interaction. The various levels of theory are employed to gain a fuller understanding of the importance of intramolecular three-electron carbon−halogen interactions, which likely affects the geometry and reactivity of one-electron-reduced DPH.

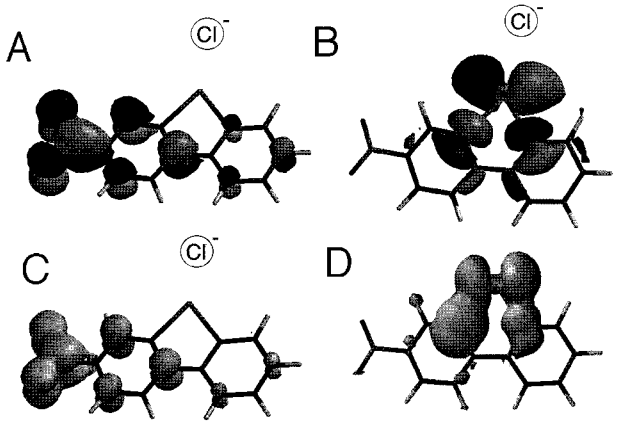

Figure 5. (A and B) LUMOs for NDPI$^+$Cl$^-$ at I−Cl distances of 2.7 Å (A) and 3.4 Å (B) calculated with DFT (pBP86/DN**). At the equilibrium geometry (A) the LUMO is in a π^*-state, whereas at the slightly increased distance in (B) a σ^*-LUMO is found. The energies of the LUMO and LUMO+1 (which are of σ^*- and π^*-symmetry, respectively, in the isolated NDPI molecule) are found to be influenced differently by the electrostatic interaction of the chloride ion. The chloride ion destablilizes the σ^*-state, allowing the π^*-unoccupied MO to become the LUMO at 2.7 Å. (C) DFT (pBP86/DN**) spin distribution for the NDPI−Cl$^{-\bullet}$ radical calculated at the geometry of the neutral species in (A). (D). DFT (pBP86 DN**) spin distribution for NDPI$^\bullet$ at the radical's optimum geometry (type AB).

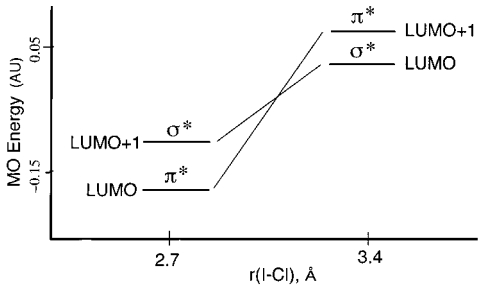

Figure 6. Unoccupied molecular orbital energies for NDPI$^+$Cl$^-$ as a function of the I−Cl distance. For NDPI$^+$Cl$^-$ with I−Cl distances beyond 3.2 Å the LUMO is of σ^* symmetry; however, as the distance decreases, the π^* state becomes more stabilized.

(a) Electronic Structure of the Parent Cations. Molecular orbital calculations were performed to establish the nature of a lowest unoccupied molecular orbital (LUMO), which is the electron accepting molecular orbital and is expected to control the early stages of the electron transfer process. Counterions were found to shift orbital energies in DPH structures so as to interchange HOMO and LUMO with the greatest effect on the NDPI orbital energies; as a consequence, the counterions were also included in calculations using chloride anion as a model. Structures were optimized at the DFT pBP/DN** level and subsequently the I−Cl interatomic distances were varied to elucidate the sensitivity of the LUMO energies in these structures to this parameter. These results were confirmed by PM3 calculations that show similar behavior.

Both DPI and NDPI without counterions show σ^*-type LUMOs. However, with a counterion at its optimized I−Cl distance of 2.68 Å we find that LUMO in NDPI is a delocalized π^*-type MO that extends to the nitro group (Figure 5A). The next vacant MO (LUMO+1) is a σ^*-type MO largely localized on iodine. Lengthening the I−Cl distance destabilizes the π^*-orbital shifting it to the higher energies (Figure 6). The σ^*-type MO becomes the lowest in energy vacant orbital in the NDPI−Cl$^-$ ion pair at the I−Cl distance exceeding 3.2 Å (Figures 5B and 6). As it might be expected, this distance is

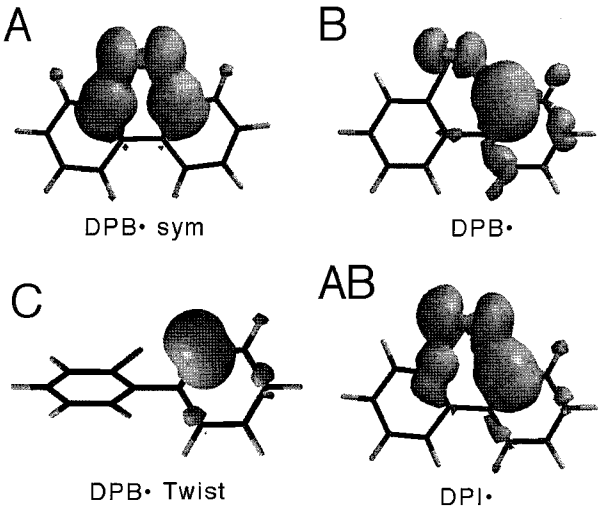

Figure 7. Spatial spin density distributions for radicals of various bonding types. Type A: symmetric structure (C_{2v}) for DPB•. Type B: asymmetric minimum energy structure for DPB•. Type C: twisted structure in which one C−Br bond is completely disrupted. Type AB: minimum energy configuration for DPI, intermediate between types A and B.

strongly affected by substituents in the aromatic core. For the DPI−Cl ion pair the $\sigma^*-\pi^*$-switch requires the chloride to approach the cation closer than 2.2 Å, that is 0.5 Å shorter and 31 kcal mol^{-1} higher in energy than in the optimized structure for this ion pair. On the other hand, further stabilization of the π^*-orbital by the second nitro group increases the π^* to σ^* I−Cl conversion distance from 3.2 Å for NDPI to 3.5 Å for DNDPI. Thus nitro groups tend to stabilize the π^*-MO over the σ^*-MO. These model calculations predict that the very nature of the primary reaction intermediate in DPH derivatives is quite sensitive to electrostatic interactions with the environment. This has important implications for the DPH derivatives intercalated into DNA, whose polyanionic backbone may control the character of LUMO in an intercalated DPH.

The effect of π-stacking similar to the one that occurs on DPH intercalation in DNA has also been tested with the result similar to the counterion effect. PM3 calculations performed with NDPI placed 3.5 Å over a single guanine base (which is the most oxidizable base in DNA)[23,24] give results that also show a stabilization of the π^*-type LUMO. However, a close inspection shows that the guanine exocyclic oxygen strongly interacts with the positively charged iodine. While this interaction is also likely dominated by electrostatics, it further demonstrates the sensitivity of the LUMO to environment in these structures. Overall, these MO calculations provide an explanation for our experimental observations for one-electron-reduced NDPI that showed a switch from the σ^*- to π^*-intermediate on intercalation into DNA (see below).

(b) One-Electron-Reduced Intermediates. Three types of structures are predicted by quantum chemical calculations for radicals formed by one-electron reduction of DPH. These structures are shown below, and their corresponding spatial electron spin distributions are shown in Figure 7. Structure A represents the hypothetical symmetric (C_{2v}) case ($r_1 = r_2$) whereas structure B is less symmetric (C_s) with $r_1 > r_2$. The distance r_1 reflects the strength of intramolecular carbon−halogen three-electron ($\sigma^2\sigma^{*1}$) bonding (see below) and approaches the length of a normal carbon−halogen bond in structure A but is longer in structure B. Structure C represents a classical 2-halobiphenyl-2′-yl radical in twisted conformation with a nonbonding r_1 distance. Table 2 reports the spin densities along with some selected geometrical parameters characterizing the structures. More detailed comparison of the structures at the DFT level is given in Table 3.

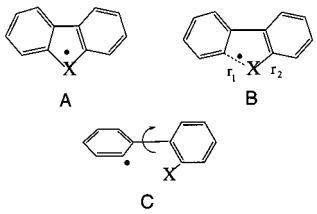

(3)

DPB•. Theoretical calculations were performed for each of the three types of structures for DPB. Optimization of DPB• at the DFT level with no symmetry restraints results in a local minimum of type B in which the spin is localized to one substantially lengthened C−Br bond ($r_1 = 2.76$ Å, $r_2 = 1.94$ Å) with a classical σ^*-type SOMO (Figure 6B). From the nature of SOMO the intermediate is classified as a $\sigma^2\sigma^{*1}$- (or simply σ^*-) radical in which most of the spin density is localized on the carbon atom (0.83) but has significant spin density on bromine (0.14); see Table 3. Our experimental estimate of the bromine spin of 0.15 compares quite favorably with this calculation and suggests this structure is that found in our experiments. Despite the obvious weakness of this interaction (reflected by the length of the C−Br bond) the σ^*-bonding overrides the substantial steric hindrance inherent in a planar structure.

Forcing the structure to maintain the C_{2v} symmetry during optimization results in a structure of type A that shows much higher spin density on the bromine (0.38) localized equally in both C−Br σ^*-bonds, which are 2.19 Å in length (Figure 7A). This structure is substantially higher in energy than the fully optimized structure (11 kcal mol^{-1} at pBP and 16 kcal mol^{-1} at B3LYP) and represents a substantial barrier to intramolecular bromine atom transfer along the σ^*-bond in structure B. DFT calculations for the fully optimized twisted geometry (C) show that this geometry is as stable as the σ^*-bonded geometry (B) at the B3LYP level and 2 kcal mol^{-1} more stable at the pBP level. This twisted structure has the spin density localized to a single carbon sp^2-type orbital with no significant spin density extended to the bromine atom (Figure 7C). PM3 calculations predict the σ^*-bonded structure B as the most stable with bond distances and spin densities similar to those found from the DFT calculations**.** On the other hand, ROHF/3-21G* calculations predict the twisted structure C as the only potential minimum. This is expected as HF-level calculations tend to underestimate σ^* bonding whereas the PM3 calculations tend to somewhat overestimate this type of bonding.

DPI•. The most stable geometry found for DPI at the DFT and PM3 levels is the AB-type structure shown in Figure 7A,B. This structure is intermediate between types A and B and characterized by comparable r_1 and r_2 distances. Substantial spin is found on the iodine (0.38) with an asymmetric spin distribution on the two carbons (0.52 and 0.07); see Table 3. There are also two local minima correspondent to structures B and C that are 1 and 5 kcal mol^{-1} higher in energy than structure AB, respectively. The large twist angle in structure C (96°) is a sign of substantial steric hindrance in a planar structure that the iodine atom provides. Clearly, the σ^*-bonding must be substantial to overcome the steric factors.

A surprising fact revealed by these calculations is that the symmetric (C_{2v}) A-type structure is located only 2 kcal mol^{-1} above structure AB. If the $r_1 = r_2$ requirement is left as the only constraint imposed on the system during optimization, the

TABLE 2: Theoretically Predicted Geometries and Halogen Spin Densities ρ(X) in One-Electron-Reduced DPHs

	UHF PM3[a]			DFT[b]			ROHF 3-21 G*	
property	DPB$^\bullet$	DPI$^\bullet$	NDPI$^\bullet$	DPB$^\bullet$	DPI$^\bullet$	NDPI$^\bullet$	DPB$^\bullet$	DPI$^\bullet$
structure	B	AB	AB	B, (C)[c]	AB	AB	C	C
ρ(X)	0.127	0.452	0.462	0.075 (0.04)	0.378	0.437	0.002	0.0003
$r(\sigma^*)$, Å[d]	2.569	2.022	2.016	2.845 (3.003)	2.546	2.457	3.323	3.993
θ, deg[e]	0.1	0.02	0.01	0.00 (30.80)	0.349	0.00	59.7	96.7

[a] Spin densities calculated at the ROHF AM1 level. [b] B3LYP/6-31G* for DPB$^\bullet$, pBP86/DN** otherwise. [c] The two energetically equivalent structures at the B3LYP/6-31G* level. [d] The length of the σ^*-bond. [e] Twist angle.

TABLE 3: DFT Results on Structure and Spin Density Distribution in One-Electron-Reduced DPH[a,b]

	ρ(X)	ρ(C1)	ρ(C2)	r_1 (Å)	r_2 (Å)	dihedral angle (deg)	DFT E (au)	rel E kcal/mol)
DPB								
DN**								
A	0.381	0.293	0.293	2.1940	2.1940	0.0000	−3036.643911	0
B	0.139	0.826	−0.009	2.7576	1.9389	0.0000	−3036.661763	−11.20
C	0.05	0.909	−0.006	3.0525	1.9364	39.4893	−3036.665356	−13.46
B3LYP								
A	0.281	0.364	0.364	2.1705	2.1705	0.0000	−3033.707497	0
B	0.075	0.927	−0.011	2.8451	1.9199	0.0000	−3033.733403	−16.26
C	0.040	0.959	−0.008	3.0035	1.9172	30.7975	−3033.734399	−16.88
DPI								
A(C_{2v})	0.467	0.251	0.251	2.3226	2.3226	0.0000	−7383.396162	2.10
A′(C_1)[c]	0.472	0.248	0.250	2.3200	2.3200	0.3604	−7383.398122	0.866
AB	0.378	0.518	0.071	2.5463	2.1925	0.3488	−7383.399502	0
C	0.001	0.961	−0.004	3.9972	2.1585	96.0881	−7383.391732	4.88
NDPI								
AB	0.437	0.429	0.104	2.4573	2.2237	0.0000	−7588.015573	
NDPB								
AB	0.155	0.806	−0.010	2.7203	1.9380	0.0000	−3241.277726	
NDPI−Cl^-[d]								
I	−0.002	−0.014	−0.061	2.1804	2.2195	0.7092	−8048.462453	
Cl	0.026							
N	0.299							

[a] All other calculations are optimizations except for restrictions noted and for NDPI−Cl^-, which is performed as a single point calculation at the geometry of the parent. [b] LSDA/pBP/DN** used for all calculations, except as noted. [c] DPI structure optimized with the sole constraint that the C−I bonds were of equal length. [d] The I−Cl distance was 3.00 Å for this calculation.

resultant structure turns out to be only 0.9 kcal mol^{-1} above structure AB. To explore this interesting observation, a series of DFT pBP/6-31G* calculations were performed in which the iodine atom was incrementally stepped in the plane of the molecule. Geometries corresponding to the minimum path through this profile were then optimized at fixed r_1 and r_2 lengths that intersected fully optimized structures. This created the single dimensional minimum energy path shown in Figure 8A. In Figure 8B several geometries found for the circle points in Figure 8A are shown. The results clearly indicate that the iodine atom is able to move between the equilibrium positions that are separated by 0.6 Å with little energy cost. These results indicate that iodine atom transfer along the σ^*-bond in the DPI radical could proceed fairly easily. If so, the real radical structure at ambient temperatures would better be represented as a dynamic equilibrium involving the pairs of equivalent AB-type and, possibly, B-type structures.

As in the case of DPB$^\bullet$, structure C represents the only potential energy minimum found for DPI$^\bullet$ at the ROHF/3-21G* level.

NDPI$^\bullet$. This system has been studied at the DFT and UHF/PM3 levels of theory with results similar to those found for DPI$^\bullet$. Full geometry optimization of the NDPI radical predicts the AB-type radical structure as the global minimum (Figure 5D); however, like DPI the potential surface is relatively flat and shows structures of type B and that of type A, which are only slightly higher in energy (this is found both at the DFT and PM3 levels). For example, at the PM3 level the largest energy difference between all three structures, A, B, and AB, does not exceed 3.5 kcal mol^{-1}. The twisted structure (C) is again found to be a local minimum about 4 kcal mol^{-1} higher (PM3) in energy than the AB-type structure. The spin densities on iodine are also essentially similar to those found for the structurally similar isomers of DPI. Thus, theoretical predictions for the isolated system agree with the experimental findings in the DMSO−ethylene glycol glass but do not agree with results found for the NDPI−DNA complex in which the spin density was found to be on the nitrogroup**.** The theoretical model for the latter system is presented below.

NDPI−Cl π^*-Radical Anion. As noted earlier, inclusion of the chloride ion was sufficient to stabilize the π LUMO in NDPI. For this reason we have performed DFT calculations for the π^*-type radical for NDPI by a single point calculation of the anion radical at the parent NDPI−Cl optimized geometry. The calculated spin density distribution shows that 70% of the spin density is localized to the nitro group, with 0.3 in the nitrogen p_z-orbital (Table 3 and Figure 5C). This is in excellent agreement with our experimental detection of a large parallel nitrogen hyperfine splitting of 27 G from the nitro group, which suggests a large spin localization on the nitrogen (ca. 0.45), as predicted by theory.

(c) Secondary Processes. The secondary transformations of phenyl-type radicals generated on one-electron reduction of cyclic halonium may involve intramolecular free radical addition

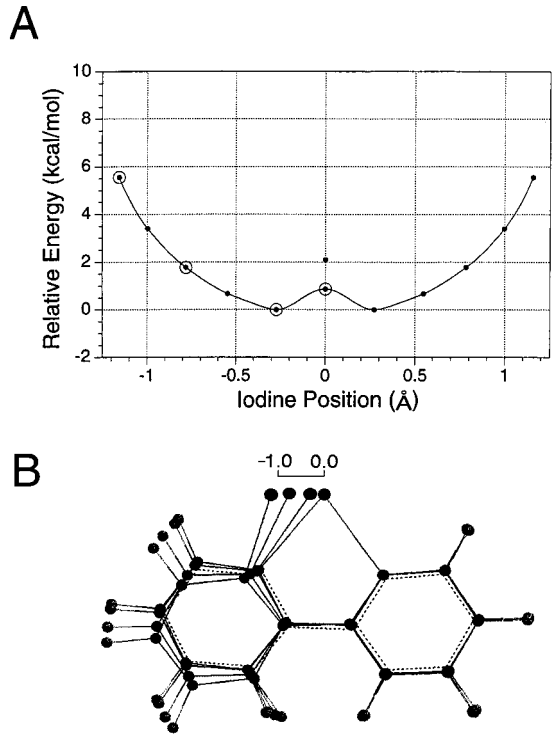

Figure 8. (A) Potential energy surface for DPI• calculated at the pBP/DFT level by moving the iodine atom along a minimum energy path away from the equilibrium geometry. (B) Structures for the circled points in (A). In (A) the two points at $x = 0$ are for the C_{2v} symmetric structure (upper point) and for the structure that restricts only the C−I bonds to be equal (lower circled point).

to the aromatic ring that leads to a cyclohexadienyl-type radical, as shown in reaction 4 for DPI. As a result, a relatively

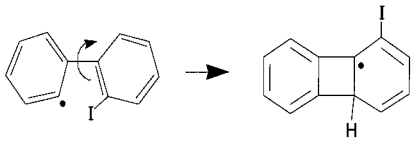

(4)

unreactive species would be formed. From the point of view of the efficiency of DPH-mediated DNA cleavage such a process would be highly undesirable since it transforms an excellent hydrogen-abstracting agent into a poor one. Calculations have been performed in order to identify the geometrical constraints capable of preventing this undesirable intramolecular process. The models selected for this theoretical study do not contain halogen atoms and, thereby, allow the use of higher levels of theory. Since spin contamination in the final doublet state was found to be a problem for these systems as well, the energies reported below have been obtained at the ROMP2/6-31G* level for the structures fully optimized at the ROHF/6-31G* level.

The systems investigated within this approach are shown in Figure 9 along with the energy changes accompanying the cyclization process. Results for the biphenyl-2-yl radical show that the cyclization leading to a strained four-membered ring is highly unfavorable, as would be expected. However, the cyclizations leading to five-membered rings are quite favorable for derivatives containing either oxygen or a carbonyl group as a linker between the phenyl rings. Thus, theoretical predictions indicate that unimolecular cyclization can compete with bimolecular hydrogen abstraction by radicals generated from six-membered halonium derivatives and, therefore, substantially reduce the yield of bimolecular reaction products. The relative rates of the intermolecular abstraction and intramolecular

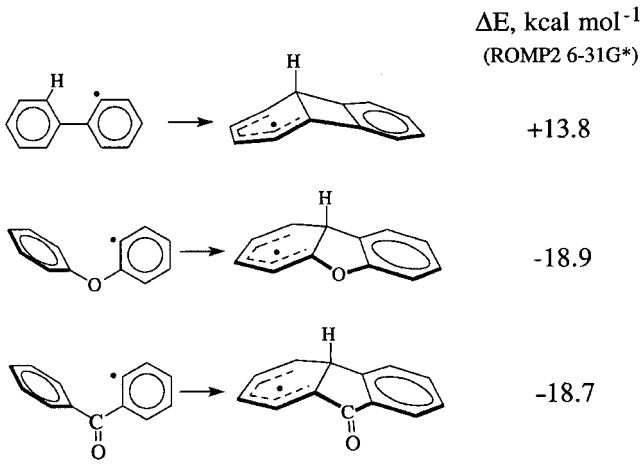

Figure 9. Theoretically predicted energy changes accompanying intramolecular formation of cyclohexadienyl-type adducts for biphenyl-2-yl free radical and related species. All structures are fully optimized at the ROHF/6-31G* level.

addition reactions would determine the effectiveness of the reduced parent molecules as DNA cleaving agents.

Discussion

Nature of the Primary Reduction Intermediate. Comparison of experimental and theoretical data leads to the conclusion that the DFT and semiempirical molecular orbital treatments provide good theoretical descriptions of one-electron-reduced DPH derivatives. Both levels of theory correctly predict the σ^* carbon−halogen bonding in the intermediates and explain the appearance of appreciable spin densities on the halogen atoms observed in the experiment. Ab initio treatments at the HF level with the limited basis sets available were not adequate to describe these species.

The theoretical prediction of a σ^*-halogen−carbon bonding in one-electron DPH establishes the basis for our use of other σ^*-bonded systems to estimate spin densities from experimental hyperfine coupling constants (Table 1). The most suitable references are the Br_2^- and I_2^- radical anions, where the spin density on the halogens ($\rho(X) = 0.5$) is known exactly for symmetry reasons. Obviously, these can only provide estimates for DPB• and DPI•, as there are differences in structure; however, the weak and localized nature of the σ^*-bonding makes these estimates reasonable ones. This approach was successfully employed previously to analyze spin density distributions in a number of other halogen-containing σ^*-bonded systems.[20,22,25−27]

Comparison of the spin densities derived from the experiment with those predicted theoretically can serve as a good test for self-consistency of the treatment. For the DPB• radical there is an excellent match between the spin densities on bromine, estimated from experiment (0.14) and those predicted by DFT (0.14) or AM1 (0.13). The estimated spin density estimated from experiment on iodine in DPI• (0.30) is between the predictions for the AB-type structure (0.40 at DFT and AM1) and the pure B-type structure (0.12). Taking into account the tendency of DFT and MNDO-based treatments to overestimate the strength of three-electron bonding, it is reasonable to conclude that the experimental spin density on the iodine in DPI• is more consistent with the more symmetrical AB-type structure.

Theoretical predictions for an isolated one-electron-reduced nitro-substituted DPI are not substantially different from those for DPI• itself, i.e., a σ^* -bonded radical with the AB-type lowest energy structure and relatively high spin density on the iodine. There is an understandable slight preference for localization of

the chiefly carbon-based free radical center in the more reducible nitro-substituted ring in the B-type isomers. However, the global energy minimum corresponds to the AB-type isomer with more equivalent C−I bonds and significantly higher spin density on the iodine (0.46 and 0.44 at the PM3 and DFT levels, respectively).

Thus, theoretical predictions for an isolated NDPI cation are consistent with the iodonium function acting as the ultimate sink for the extra electron added upon reduction**.** This agrees with the σ*-type intermediate generated from NDPI in the DMSO-ethylene glycol matrix, which is very similar to the intermediates observed for DPI and for amino-substituted DPIs. However, the intermediate generated from NDPI intercalated into DNA dramatically differs from the one observed in polar glasses. Localization of spin density in the nitro group of one-electron-reduced NDPI intercalated into DNA indicates the π*-type SOMO originating from the π*-LUMO of the parent cation shown in Figure 5A. In terms of charge distribution this means a bipolar intermediate with the negatively charged nitro group and electropositive iodine:

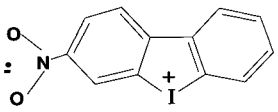

(5)

The influence of DNA on the nature of electronic state in one-electron-reduced NDPI can be rationalized by our theoretical findings that the "vertical" electron attachment to the π*-LUMO of an NDPI−counterion pair produces a bipolar π*-radical intermediate, which relaxes on annealing to the less polar σ*-state**.** Furthermore, the π*−σ*-relaxation in NDPI$^{\bullet}$ is actually a case of intramolecular electron transfer, which must include internal and external (solvent) reorganization energies. As a consequence an activation energy for this process is expected.

The electrostatic field appears to be an important factor that controls the nature of the SOMO in NDPI$^{\bullet}$. Theoretical calculations show that the σ* state is found in weak fields and the π* state is found in stronger fields. Supporting evidence is found from our experimental work. In the polar DMSO−ethylene glycol glass the solute likely exists as a solvent-separated ion pair in which the NDPI cation is much less affected by the field of the anion. The σ*-LUMO is found in this medium immediately after electron attachment, as found for other DPI derivatives. The π* state is found only when NDPI$^{\bullet}$ is intercalated in DNA. In this case the DNA polyanionic backbone provides a substantial electric field that is able to stabilize the π*-state.

In conclusion, a σ*-type radical best describes one-electron-reduced diphenylenehalonium radicals based on both theoretical calculations and experimental results. Consideration of these radicals as examples of hypothetical diarylhalogen species, $Ar_2X^{\bullet}$, is chiefly a matter of terminology. However, for DPB$^{\bullet}$ the clear disadvantage of such a formulation is that it does not reflect the real electronic structure and strong nonequivalence of the C−X bonds in DPH radicals. From the spin density distribution and bond lengths standpoints, DPB$^{\bullet}$ is a fairly weakly bound intramolecular σ*-complex of a phenyl-type radical. The case is similar for DPI$^{\bullet}$, but the somewhat stronger σ*-bonding makes this structure closer to that expected for hypothetical diaryliodine species. The motion of the iodine atom in DPI radicals is found to be surprisingly facile. Calculations suggest the iodine atom can move about 1.6 Å with only 2 kcal mol^{-1} of energy. Moreover, the predicted low potential barrier (1−2 kcal mol^{-1}) between the equivalent AB-type structures in DPI$^{\bullet}$ would make the two C−I bonds effectively equivalent on a reaction time scale.

Since no results attributable to the $Ar_2I^{\bullet}$ species have been detected on one-electron reduction of acyclic diphenyliodonium cations even in low-temperature glasses, the five-membered ring structure plays a crucial role in stabilization of the σ*-bond in DPH radicals. A similar stabilizing effect of five-membered and, more rarely, of a six-membered ring formation on the σ*-bonds has long been recognized for isoelectronic σ*-bonded sulfuranyl radicals $R_3S^{\bullet}$.[8]

The near degeneracy of σ*- and π*-MOs in the nitro-substituted DPI, i.e., NDPI, create an unusual system that is highly sensitive to environment, so that at low temperatures the σ*-state is found in polar glasses whereas the π*-state is found in DNA as a metastable state (discussed below).

Chemical Reactivity of DPH Radicals. An obvious consequence of the σ*-bonding in the DPH radicals should be some reduction in their reactivity in hydrogen atom transfer reactions compared to a free phenyl radical. The practically important question pertinent to DNA-cleaving ability of DPH is whether this reduction will still allow the DPH radicals to remain reasonably good hydrogen-abstracting agents. Quantitatively, the difference in reaction enthalpies for hydrogen abstraction by a classical biphenyl-2-yl radical and a DPH radical is the enthalpy of the σ*-bond formation in the latter. The C−H energy in benzene is 110 kcal mol^{-1}, while the weakest C−H bonds in the deoxyribose moiety of DNA have energies around 90 kcal mol^{-1}.[28] Thus hydrogen abstraction from DNA by a classical phenyl radical should be exothermic by almost 20 kcal mol^{-1}. Since the strength of the σ*-bond in DPH radicals appears to be much below this value, energetically these species should still remain good hydrogen-abstracting agents. This prediction fully agrees with earlier experiments[1] in which DPH radicals were still be able to abstract hydrogen from DNA. However, unlike phenyl radicals, DPH radicals can be easily trapped in a reactive ethylene glycol glass at 77 K. The question that still remains is whether hydrogen abstraction by DPH$^{\bullet}$ requires formation of a more reactive form (such as the twisted form) of these radicals:

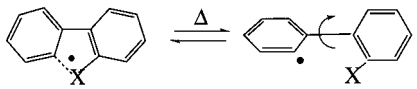

(6)

Even if energetically possible, the direct hydrogen abstraction by the σ*-bonded isomer is likely to be complicated by steric hindrance in the transition state and, therefore, would require a higher activation energy. This can make the direct abstraction noncompetitive with the process that goes through the classical phenyl-type free radical.

Even higher thermal stability is displayed by the π*-type intermediate generated by irradiation of NDPI intercalated into DNA. This species does not seem to react with the DNA host in a frozen aqueous medium. This is not unusual since π*-radical anions of nitroaromatic compounds are known for their stability. However, in fluid solutions NDPI was found to cleave DNA like other DPH derivatives and to form iodonitrobiphenyls as the stable reaction products, which is consistent with hydrogen atom transfer to a σ*-intermediate.[6] This indicates that on annealing the π*-radical intermediate undergoes π*- to σ*-conversion, leading to the σ*-intermediate, which acts as a hydrogen abstractor. This state likely develops by a suitable alteration in environment on annealing.

Conclusions

One-electron reduction of *o,o′*-diphenylenebromonium cations and their iodonium analogues in glassy matrixes results in production of partially halogen-centered radicals as the primary reaction intermediates. Formally, these reduction products can be considered as the first direct spectroscopic detection of diarylbromine and diaryliodine species $Ar_2X^{\bullet}$, whose existence has long been assumed on the basis of circumstantial data. However, the halogen spin densities estimated using the ESR technique from experimental hyperfine couplings with halogens and from molecular-orbital calculations show that DPB$^{\bullet}$ radical is better represented as the ≡C$^{\bullet}$···Br−C≡ free radical complex with localization of most of the spin density on the sp^2-carbon atom. In other words, this species is in fact the example of weak intramolecular σ^*-complexes formed by phenyl-type radicals with halogenated benzene compounds. The case for DPI$^{\bullet}$ differs in that the C−I bond lengths are more nearly equivalent and the spin density is found on both carbon atoms. In addition, the very low barriers for intramolecular iodine migration predicted for DPI$^{\bullet}$ allow a fast iodine exchange between equilibrium positions in the molecule. Such a dynamic process could result in effective equivalence of the C−I bonds on a chemical time scale. Chemically, both complexes are excellent hydrogen abstractors with somewhat reduced reactivity compared to the phenyl radical. The geometrical constraints associated with their five-membered cyclic structure is crucially important for stability of these complexes, since no such intermediates can be detected upon one-electron reduction of the diphenyliodonium cation.

Finally, both experiment and theory agree that the symmetry of the SOMO in NDPI$^{\bullet}$ shows a remarkable sensitivity to environment. In our experimental work NDPI$^{\bullet}$ changes its character from σ^* in a solution to π^* when complexed in DNA. Our MO calculations agree with experiment and show that NDPI$^{\bullet}$ in the gas phase would be in the σ^*-state, as found for DPI$^{\bullet}$. However, the calculations show that when a counterion is present or when a single guanine is stacked 3.5 A above NDPI$^{\bullet}$, this radical converts to the π^*-state.

Acknowledgment. We thank the National Cancer Institute of the National Institutes of Health (Grant RO1CA45424) and the Oakland University Research Excellence Fund for support of this work.

References and Notes

(1) Razskazovskii, Y.; Roginskaya, M.; Sevilla, M. D. *Radiat. Res.* **1998**, *149*, 422−432.

(2) von Sonntag, C. *The Chemical Basis of Radiation Biology*; Taylor, Francis: London, New York, Philadelphia, 1987; pp 1−240.

(3) Zimbrick, J. D.; Ward, J. F.; Myers, L. S., Jr. *Int. J. Radiat. Biol.* **1969**, *16*, 525−534.

(4) Zimbrick, J. D.; Ward, J. F.; Myers, L. S., Jr. *Int. J. Radiat. Biol.* **1969**, *16*, 505−523.

(5) Pogozelski, W. K.; Tullius, T. D. *Chem. Rev.* **1998**, *98*, 1089−1107.

(6) Razskazovskii, Y. V.; Sevilla, M. D. Results in preparation for publication.

(7) Dekeijzer, A. E. H.; Buck, H. M. *Phosphorus Sulfur* **1987**, *31*, 203−214.

(8) Margaretha, P. In *S−Centered Radicals*; Alfassi, Z. B., Ed.; John Wiley Sons: New York, 1999; pp 277−288.

(9) Yagci, Y.; Pappas, S. P.; Schnabel, W. *Z. Naturforsch. A* **1987**, *42*, 1425−1427.

(10) Welsh, K. M.; Dektar, J. L.; Garciagaribaya, M. A.; Hacker, N. P.; Turro, N. J. *J. Org. Chem.* **1992**, *57*, 4179−4184.

(11) Geahigan, K. B.; Taintor, R. J.; George, B. M.; Meagher, D. A.; Nalli, T. W. *J. Org. Chem.* **1998**, *63*, 6141−6145.

(12) Nesmeyanov, A. N.; Lisichkina, I. N.; Vanchikov, A. N.; Tolstaya, T. P. *Doklady Akademii Nauk SSSR* **1976**, *228*, 99−101.

(13) Collette, J.; McGreer, D.; Crawford, R.; Chubb, F.; Sandin, R. B. *J. Am. Chem. Soc.* **1954**, *78*, 3819−3820.

(14) Wasylewsky, A.; Brown, R. K.; Sandin, R. B. *J. Am. Chem. Soc.* **1950**, *72*, 1038−1039.

(15) Beringer, F. M.; Kravetz, L.; Topliss, G. B. *J. Am. Chem. Soc.* **1965**, *30*, 1141−1147.

(16) Frisch, M. J., et al. Gaussian, Inc.: Pittsburgh, PA, 1995.

(17) Hehre, W. J.; Lou, L. A. *Guide to Density Functional Calculations in SPARTAN*; Wavefunction, Inc.: Irvine, CA, 1997.

(18) Tolkachev, V. A.; Chkheidze, I. I.; Buben, N. Y. *Zh. Strukt. Khim.* **1962**, *3*, 709.

(19) Adrian, F. J.; Cochran, E. L.; Bowers, V. A. *J. Chem. Phys.* **1962**, *36*, 1661.

(20) Champagne, M. H.; Mullins, M. W.; Colson, A.-O.; Sevilla, M. D. *J. Phys. Chem.* **1991**, *95*, 6487−6493.

(21) Boesman, E.; Schoemacher, J. *J. Chem. Phys.* **1962**, *37*, 671.

(22) Sevilla, M. D.; Summerfield, S.; Eliezer, I.; Rak, J.; Symons, M. C. R. *J. Phys. Chem. A* **1997**, *101*, 2910−2915.

(23) Colson, A.; Besler, B.; Sevilla, M. D. *J. Phys. Chem.* **1992**, *96*, 9787−9794.

(24) Steenken, S.; Jovanovic, S. V. *J. Am. Chem. Soc.* **1997**, *119*, 617−618.

(25) Abu-Raqabah, A.; Symons, M. C. R. *J. Chem. Soc., Faraday Trans.* **1990**, *86*, 3293.

(26) Abu-Raqabah, A.; Symons, M. C. R. *J. Am. Chem. Soc.* **1990**, *112*, 8614.

(27) Raynor, J. B.; Rowland, I. J.; Symons, M. C. R. *J. Chem. Soc., Faraday Trans.* **1991**, *87*, 571.

(28) Colson, A. O.; Sevilla, M. D. *J. Phys. Chem.* **1995**, *99*, 3867−3874.